10.24425/acs.2025.157237

Archives of Control Sciences
Volume 35(LXXI), 2025
No. 4, *pages* 835–861

Controllers design for time-delay systems and analysis of robustness limits of iso-damping property with experimental validation

Mourad ALLAD, Moussa CHARIF and Nadir FERGANI

Although the field of fractional-order control (FOC) has seen significant progress, the key benefit of this strategy lies in achieving an iso-damped system. Preserving this robustness property in time-delay systems remains highly challenging and requires precise quantification to properly evaluate controller robustness with respect to plant static gain variations.

This paper investigates the limitations of achieving iso-damping in lag-dominated timedelay systems. To address this challenge, a comparative study of three analytical design methods for FOC is conducted, with particular emphasis on iso-damping preservation. New frequency-domain robustness metric is proposed, quantifying the deviation between the open-loop response and the Bode's Ideal Transfer Function (BITF). The analysis and experimental validation, on level control system stand, reveal that iso-damping performance deteriorates as time delay increases, with the degree of degradation depending strongly on controller structure and tuning strategy. Moreover, the results confirm a robustness boundary defined by the condition $\theta.\omega_c < 0.5$, beyond which iso-damping cannot be reliably maintained. While all methods satisfy initial design specifications, only one consistently preserves robustness across a wide range of time delays. These results highlight a fundamental trade-off between bandwidth and robustness, underscoring the importance of careful controller design in time-delay systems.

Key words: Fractional-Order Proportional-Integral-Derivative controller (FOPID), flat phase, iso-damping, first order plus time delay (FOPTD) system, robustness index; level and flow control

M. Allad (corresponding author, e-mail: mourad.allad@ummto.dz) and M. Charif (e-mail: moussa.charif@ummto.dz) are with Laboratoire Vision Artificielle et Automatique des Systèmes (LVAAS), Automatic Department, Faculty of Electrical Engineering and Computer Science, Tizi-Ouzou University, Algeria.

N. Fergani (e-mail: n.fergani@crti.dz) is with Research Center in Industrial Technologies CRTI, P.O. Box 64, Cheraga, Algiers, 16014, Algeria.

Received 26.08.2025.

1. Introduction

Fractional calculus has attracted increasing attention in control engineering since its introduction by Oustaloup via the well-known CRONE controller (Commande Robuste d'Ordre Non Entier) [1], which applies fractional-order operators to control both integer and non-integer order systems. The introduction of the FOPID controller by Podloubny [2], as a generalization of the classical PID, marked a major advancement by enhancing the flexibility of the controller in shaping dynamic behavior and improving robustness for model uncertainties. Since then, fractional-order control has become a broad research topic, and a major research direction has focused on the design and tuning of fractional-order controllers. Numerous studies have proposed synthesis and tuning methods seeking to exploit the advantages of this control strategy in terms of performance and robustness [3–5].

Fractional order control (FOC) design methods are generally classified into two main categories. The first one is numerical or optimization-based design , where the objective is to optimize the time domain specifications as demonstrated in [6, 7] or frequency domain specifications as in [8, 9]. The second category is analytical design, which typically employs a frequency domain approach or considers a desired closed-loop transfer function as in [10–13]. The most used desired model is the Bode's ideal transfer function (BITF), being the first application of fractional calculus in control engineering [1, 14, 15]. Although many studies have been published over the past three decades, a key advantage of fractional-order controllers remains their ability to achieve the iso-damping property, which signifies insensitivity to static gain variations. This characteristic, inspired by the Bode's Ideal Transfer Function (BITF), is attained when the open-loop system exhibits a flat phase near the unity gain crossover frequency.

For stable linear delay-free systems, the iso-damping property has been easily achieved in various studies [1, 12, 16]. On the other hand, the open-loop phase decreases with frequency in presence of pure time-delay, limiting the flat phase to a narrow frequency band. In addition to the well-known bandwidth limitation imposed by the time delay [17], the design of a robust iso-damped loop for lag-dominated time-delay systems presents a significant challenge for control engineers.

From the literature, many works have achieved the iso-damping property for time-delay systems. Two main approaches can be identified in this context. The first involves ensuring a minimum slope of the phase curve at the unity gain crossover frequency, based on the well-known condition $d(\arg)/d\omega = 0$ proposed in [18]. This condition has been used in several studies [8, 11, 15, 19–22], achieving

a flat phase over a limited frequency band for various controller structures. These include the FOPID structure [8], PI$^{\lambda}$ [19,22], PD$^{\mu}$ [21], [PD]$^{\mu}$ [15], PI$^{\lambda}$D [11] and implementations combined with a filter [20]. The second approach involves using the BITF as a reference model, from which the controller parameters are derived either through a time optimization approach as in [6], or by the design of the closed loop transfer function to be equivalent to the desired model as in [10], where a model-based controller was designed using the IMC technique. In [23], this approach was extended by introducing a new time-delay approximation, which enhances the phase flatness region compared to [10]. More recently, in [24], a fractional-order active disturbance rejection control (FO-ADRC) scheme was proposed to design an iso-damped system. While this method enhances robustness to gain variations, its phase flatness property was shown to degrade when applied to the FOPTD processes.

Another analytical idea was proposed in [25], where the delayed BITF is considered as the reference model. However, the drawback of this approach is that the phase flatness is partially lost when this reference model is used.

Although numerous studies have addressed time delay systems, the flat phase property remains limited to a narrow frequency band, which varies depending on the method employed. Analytical tuning methods of FOC remain limited, particularly regarding experimental validation. Moreover, the robustness to static gain variation differs across controllers designed using various approaches, highlighting the need to quantify the iso-damping through a standard index.

The present work primarily aims to investigate the effect of time-delay on the iso-damping property, with particular emphasis on the limitation it imposes on the bandwidth. A novel frequency-domain robustness index is proposed to quantify the degree of iso-damping robustness among different controllers. A comparative study with experimental validation of three analytical design methods of the fractional order controller has been carried out in order to validate theoretical approaches. It is worth noting that most previous studies using fractional order controllers for liquid level processes did not consider the flat phase property [26–28], except for the optimization based design presented in [8].

The remainder of this paper is structured as follows: Section 2 describes the liquid level and flow apparatus, detailing its various components and presenting the system identification. Section 3 demonstrates the principles of three analytical tuning methods for fractional-order controllers that achieve the iso-damping property. Section 4 presents the proposed robustness evaluation index. Section 5 presents simulation and experimental results in both time and frequency domains for the different controllers applied to time-delay systems. Finally, concluding remarks are provided in Section 6.

2. Description of laboratory test stand

The experimental setup used in this study is a liquid level and flow control system (Fig. 1), representative of a class of the FOPTD process often found in industrial applications. The system is located at the Control Laboratory of the Department of Automation and consists of the following main components (Table 1).

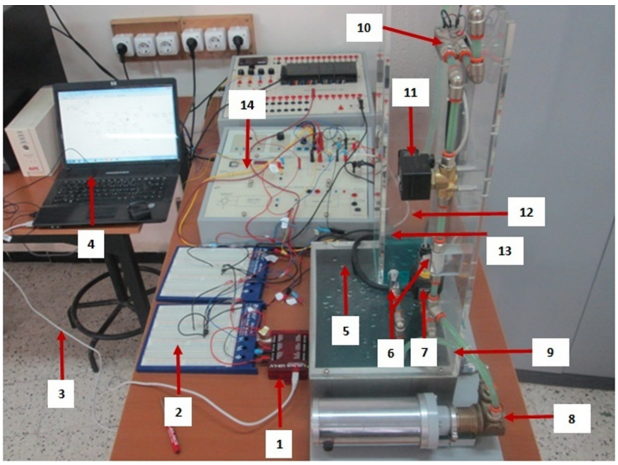

Figure 1: Experimental test bench components

Table 1: Components of the Liquid Level Control System

1: LabJack U3-LV	2: Adaptation of the signals	3: USB cable	4: Laptop
5: Reservoir	6: Hand valve	7: On/Off valve	8: Pump
9: Pipe	10: Flow sensor	11: Proportional valve	12: Tank
13: Level sensor	14: Panel of the level & flow transmitters, supply and control		

According to Fig. 1, the proportional valve is presented by element (11), the objective of which is to control liquid level in the tank (12). This stand has been used to validate various advanced control strategy as in [29] and [30].

2.1. Process identification

The first task of this work is to determine the transfer function of the system around the operating point. To achieve this, the static characteristic of the process was first obtained, followed by the selection of a linear operating region. The working point was selected at an input voltage equal to $u_1 = 5$ V, corresponding to an output level voltage $y_1 = 2.42$ V. Subsequently, a step input was then

applied by increasing the input from 5 V to 6 V and the resulting system response was recorded. The resulting step response exhibited first-order dynamic with the resulting steady-state $y_2 = 7.07$ V.

According to this step response, we can determine the model parameters. For that, the Broïda method has been used.

- Static gain

$$K = \frac{7.07 - 2.42}{6 - 5} = 4.65. \tag{1}$$

- Constant time: $\tau = 157$ s.
- Delay time $\theta = 3$ s.

The transfer function can be expressed by:

$$G(p) = \frac{4.65}{157s + 1} e^{-3s}. \tag{2}$$

3. Controller design techniques

This section presents three analytical methods for designing fractional-order controllers intended to achieve the iso-damping property for time-delay systems. Each method is based on a different design philosophy and mathematical formulation. The selected approaches include:

- **Method 1** [11]: An optimal robust FOPID controller design based on phase flattening condition near the crossover frequency.
- **Method 2** [10]: A model-based FOPID controller derived from the Bode's Ideal Transfer Function (BITF) using frequency response matching and Internal Model Control (IMC) principles.
- **Method 3** [23]: A direct synthesis FOPID controller designed using a new time delay approximation, developed to enhance the phase flatness region.

For each method, the controller parameters are derived analytically, and the resulting open-loop characteristics are evaluated to ensure the preservation of iso-damping behavior. The methods are then compared based on time-domain and frequency-domain responses, as well as robustness metrics.

The functional block diagram is shown in Fig. 2.

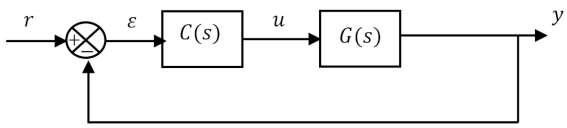

Figure 2: Conventional feedback control

r and y are the input and output actual signals, respectively, ε, u are the error signal and controller output. The first order plus time-delay has been considered in this work.

$$G(s) = \frac{K}{1+\tau s} e^{-\theta s}. \tag{3}$$

The desired loop is represented in Fig. 3.

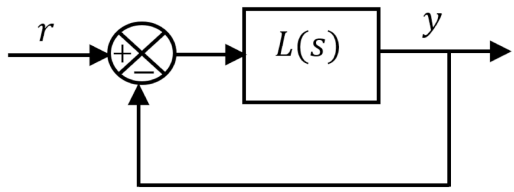

Figure 3: Bode's ideal loop

The ideal open-loop transfer function, often referred to as Bode's Ideal Transfer Function (BITF), is defined as:

$$L(s) = \frac{1}{\left(\frac{s}{\omega_c}\right)^m}, \tag{4}$$

ω_c is the gain crossover frequency and this system includes several dynamics behaviors depending on its fractional order m. When $1 < m < 2$, system exhibits an under-damped or oscillatory response.

In the Bode diagram, the magnitude of $L(s)$ is a straight line with constant slop of -20 mdB/dec, and its phase curve is a horizontal line at $-20m\pi/2$ rad, which indicates that $L(s)$ has important robustness against the static gain variation (called the iso-damping property) where the phase is independent to the gain crossover frequency.

3.1. Method 1: Optimal robust FOPID controller design

An optimal robust FOPID controller for the FOPTD process proposed by [11, 19]. The method considers both frequency-domain (FD) specifications and time-domain (TD) requirements. Furthermore, the paper presents simulation results. A summary of the principle of the method is presented below.

GMPT (gain phase margin tester) in series with $C(s)$ is applied to plot the parameter boundaries of the controller with the $PM(\Phi)$ and gain margin (A).

$$M_T(A, \Phi) = Ae^{-j\Phi}. \tag{5}$$

In this case, keeping $A = 1$ and with different Φ, the controller parameters satisfying $PM(\Phi_m) = \Phi$ can be obtained.

$C(s)$ is the proposed (FOPID) controller as below:

$$C(s) = K_p + \frac{K_i}{s^\lambda} + K_d s, \tag{6}$$

where K_p, K_i and K_d are proportional, integral, and derivative gains, respectively. $\lambda \in (0, 2)$.

The characteristic equation of the control system is:

$$D\left(s : K_p, K_i, \lambda, K_d, A, \Phi\right) = s^\lambda(\tau s + 1) + \left(K_p s^\lambda + K_i + K_d s^{\lambda+1}\right) \times A e^{-j\Phi} e^{-\theta s}. \tag{7}$$

The stability region boundaries can be illustrated by real root boundary (RRB: the boundary of K_i is $K_i = 0$), infinite root boundary $\left(\text{IRB} : K_d = \mp\frac{\tau}{K}\right)$ and complex root boundary (CRB) as follows:

$$D\left(j\omega\colon K_p, K_i, \lambda, K_d, A, \Phi\right) = (j\omega)^\lambda(\tau j\omega + 1) + \left(K_p(j\omega)^\lambda + K_i + K_d(j\omega)^{\lambda+1}\right) \times A e^{-j\Phi} e^{-\theta j\omega} = 0. \tag{8}$$

The real and imaginary parts are:

$$\begin{cases} B_1 + AKC_1E + AKS_1F = 0, \\ B_2 + AKC_1F + AKS_1E = 0, \end{cases} \tag{9}$$

$$C_1 = \cos\left(\Phi + \omega\theta\right), \quad C_2 = \cos\left(\frac{\lambda\pi}{2}\right), \quad C_3 = \cos\left(\frac{(\lambda+1)\pi}{2}\right),$$

$$S_1 = \sin\left(\Phi + \omega\theta\right), \quad S_2 = \sin\left(\frac{\lambda\pi}{2}\right), \quad S_3 = \sin\left(\frac{(\lambda+1)\pi}{2}\right),$$

$$B_1 = \omega^\lambda C_2 - \tau\omega^{\lambda+1}S_2, \quad B_2 = \tau\omega^{\lambda+1}C_2 + \omega^\lambda S_2,$$

$$E = K_p\omega^\lambda C_2 + K_i + K_d\omega^{\lambda+1}C_3, \quad F = K_p\omega^\lambda S_2 + K_d\omega^{\lambda+1}S_3.$$

After solving the equation (9), the K_p and K_i are:

$$K_p = \frac{-\left(B_1S_1 + B_2C_1\right)}{AKS_2\omega^\lambda} - \frac{K_d\omega S_3}{S_2}, \tag{10}$$

$$K_i = \left(B_2 - \frac{B_1C_1}{S_1}\right)\frac{1}{\left(AKS_1 + AKC_1^2/S_1\right)} - K_p\omega^\lambda C_2 - K_d\omega^{\lambda+1}C_3. \tag{11}$$

After introduction of ω_c, Φ_m, K_d and λ, the other two parameters K_p and K_i can be fixed. Sweeping over the λ in $(0, 2)$ a curve named as relative stability curve (RSC) can be obtained.

Three (FD) specifications Φ_m, ω_c, and flat phase constraints are applied to design the FOPID controller.

$$\frac{d\Phi_m}{d\omega_c} = 0. \tag{12}$$

The flat phase constraint (FPC) is applied to design the FOPID controller to make the system robust to the loop gain variations. From Eq. (9)

$$S_1 = \frac{B_2E - B_1F}{AK(E^2 + F^2)}, \tag{13}$$

$$C_1 = \frac{-B_1E - B_2F}{AK(E^2 + F^2)}, \tag{14}$$

$$\Phi = \arctan\left(\frac{B_1E - B_2F}{B_1E + B_2F}\right) - \omega\theta - n\pi. \tag{15}$$

To satisfy the phase Bode plot is flat at ω_{gc}:

$$\frac{d\Phi}{d\omega} = \frac{\left(B_1^2 - B_2^2\right)\left(EF' - E'F\right) + \left(B_1'B_2 - B_1B_2'\right)\left(E^2 + F^2\right)}{\left(B_1E + B_2F\right)^2 + \left(B_1F + B_2E\right)^2}. \tag{16}$$

Sweeping all the K_d from $\left(\frac{-\tau}{K} \text{ to } \frac{+\tau}{K}\right)$ one curve named (FPC) can be obtained. All the points on FPC can ensure the three specifications ω_c, Φ_m, and flat phase.

The parameters of the FOPID controller corresponding to the points on the PFC, the ITAEs are calculated after simulation the step responses.

The integral time absolute error ITAE has been used to obtain the optimal dynamic performance:

$$J_{ITAE} = \int_0^\infty t\,|\varepsilon(t)|\,\mathrm{d}t. \tag{17}$$

The smallest J_{ITAE} must be chosen to determine the parameters of the FOPID controller.

3.2. Method 2: IMC-PID-fractional-filter controller design

This method is based on IMC approach where the design procedure aims to match the closed-loop frequency response with a desired model, typically the Bode's Ideal Transfer Function (BITF), while addressing time-delay effects through an appropriate approximation (Padé approximation) [10].

According to Eq. (4) of Bode's ideal transfer function, we impose: $\tau_c = \frac{1}{\omega_c^\alpha}$; $\alpha = m$. The IMC functional block diagram is shown in Fig. 4.

y_m in Fig. 4 represents the model response and y is the plant response.

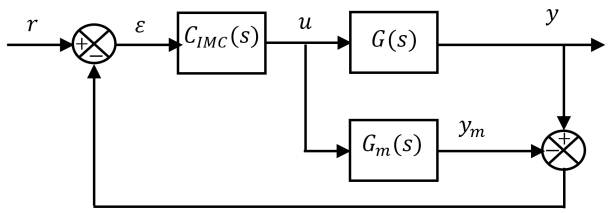

Figure 4: Internal model control structure

The block diagram for the conventional feedback control is given in Fig. 2. It can be shown that the two block diagrams are identical if controllers $C(s)$, and $C_{IMC}(s)$ satisfy the relation:

$$C(s) = \frac{C_{IMC}(s)}{1 - C_{IMC}(s)G_m(s)}. \tag{18}$$

For the special case of a perfect model $G_m(s) = G(s)$, the output y obtained:

$$y = C_{IMC}Gr. \tag{19}$$

The controller design procedure for the proposed method is summarized as follows:

- Step 1: According to the IMC controller design. $G_m(s)$ must be factorized as:

$$G_m(s) = G_m^+(s)G_m^-(s), \tag{20}$$

  where $G_m^+(s)$ contains any time delays and right half plane zeros. $G_m^+(s)$ must have a steady-state gain equal to one.

- Step 2: The controller is specified as:

$$C_{IMC}(s) = \frac{1}{G_m^-(s)} f(s), \tag{21}$$

  $f(s)$ is a low pass filter with a steady-state gain of one. The fractional property of the controller is introduced by the fractional reference $f(s)$ to obtain iso-damping. $f(s)$ is given by:

$$f(s) = \frac{1}{1 + \tau_c s^{\alpha+1}}; \quad 0 < \alpha < 1, \tag{22}$$

  where τ_c and the non-integer α are chosen to impose the phase margin $\emptyset_m$ and the crossover frequency ω_c of the closed-loop

$$\alpha = \frac{\pi - \emptyset_m}{\pi/2} - 1 \wedge \tau_c = \frac{1}{\omega_c^{\alpha+1}}. \tag{23}$$

- Step 3: The IMC controller is calculated by Eq. (23).
- Step 4: The standard feedback controller is:

$$C(s) = \frac{C_{IMC}(s)}{1 - C_{IMC}(s)G_m(s)}\,. \tag{24}$$

- Step 5: The controller $C(s)$ can be put in the form of an integer PID structure cascaded with a fractional filter.

$$C(s) = \underbrace{H(s)}_{\text{Fractional filter}} \cdot \underbrace{K_p\left(1 + \frac{1}{T_i s} + T_d s\right)}_{\text{Integer PID controller}}. \tag{25}$$

Padé approximation of the $e^{-\theta s}$ is given by:

$$e^{-\theta s} = \frac{1 - \frac{\theta}{2}s}{1 + \frac{\theta}{2}s}\,. \tag{26}$$

Substituting the time delay approximation in $G_m(s)$ and using Eq. (21), the IMC controller is:

$$C_{IMC}(s) = \frac{(1 + \tau s)\left(1 + \frac{\theta}{2}s\right)}{K(1 + \tau_c s^{\alpha+1})}\,. \tag{27}$$

Thus, the corresponding feedback controller is:

$$C(s) = \frac{(1 + \tau s)\left(1 + \frac{\theta}{2}s\right)}{K\left(1 + \tau_c s^{\alpha+1} + \frac{\theta}{2}s\right)} = \frac{1 + \frac{2\tau + \theta}{2}s + \frac{\tau\theta}{2}s^2}{\frac{K\tau}{2}s\left(1 + \frac{2\tau_c}{\tau}s^{\alpha}\right)}\,. \tag{28}$$

The controller can be written as Eq. (25):

$$H(s) = \frac{1}{1 + \frac{2\tau_c}{\theta}s^{\alpha}}; \quad K_p = \frac{2\tau + \theta}{K\theta}; \quad T_i = \frac{2\tau + \theta}{2}; \quad T_d = \frac{\tau\theta}{2\tau + \theta}\,. \tag{29}$$

3.3. Method 3: Direct synthesis controller

This method is based on the direct synthesis approach, wherein the fractional order (FOPID) controller cascaded with a first order lead compensator which are used to control the FOPTD process [23].

The desired closed-loop transfer function $G_d(s)$ is given from Eq. (4).

$G(s)$ and $C(s)$ are the transfer function of the plant and the FOPID, respectively.

$$G(s) = G_f(s)e^{-\theta s}, \tag{30}$$

$G_f(s)$ is the delay-free process.

To design a closed-loop system that has the iso-damping property, it is necessary to satisfy the following desired open loop transfer function:

$$L(s) = C(s)G_f(s)e^{-\theta s} \approx \frac{1}{\left(\frac{s}{\omega_c}\right)^m}. \tag{31}$$

The proposed controller is composed of two cascading parts as:

$$C(s) = C_m(s)C_n(s). \tag{32}$$

The open loop transfer function is designed as:

$$\underbrace{\left(C_m(s)G_f(s)\right)}_{\approx\frac{1}{\left(\frac{s}{\omega_c}\right)^m}}\underbrace{\left(C_n(s)e^{-\theta s}\right)}_{\approx 1} \approx \frac{1}{\left(\frac{s}{\omega_c}\right)^m}. \tag{33}$$

The first part $C_m(s)$ is the fractional order controller that satisfies the Bode's ideal open loop for the delay-free system $G_f(s)$ and the second part $C_n(s)$ is a rational minimum phase transfer function that compensates the time delay effect around the specific point $s = j\omega_c$.

The controller is designed as follows:

- Design the minimum phase approximation of the pure time delay $f(s) \approx e^{-\theta s}$ then, the compensator $C_n(s)$ is obtained as:

$$C_n(s) = \frac{1}{f(s)}, \tag{34}$$

$$f(s) = g\left(\frac{1+as}{1+bs}\right); \quad \text{with} \quad b > a. \tag{35}$$

This transfer function is a lag compensator which gives a negative phase in a specific frequency band (inferior to $-45°$ in $\left[\frac{1}{b}\frac{1}{a}\right]$. Indeed, the pure time delay system $e^{-\theta s}$ can be approximated around the specific point $s = j\omega_c$ by the rational

minimal phase transfer (35), where the three parameters a, b and g are given by:

$$\begin{aligned} &\frac{1}{a} \gg \omega_c\,, \\ &b = \frac{1}{\omega_c}\tan\left\{\tan^{-1}(a\omega_c) + \theta\omega_c\right\}, \\ &g = \frac{\sqrt{1+\tan^2\left\{\tan^{-1}(a\omega_c)+\theta\omega_c\right\}}}{\sqrt{1+(a\omega_c)^2}}\,. \end{aligned} \tag{36}$$

In order to obtain the same phase slope, the specific frequency ω_c must be chosen with the following condition:

$$\theta\omega_c \leqslant 0.5.$$

- Design the controller $C_m(s)$ for the delay-free system as follows:

From equation (33), the controller $C_m(s)$ is:

$$C_m(s) = \frac{1}{\left(\dfrac{s}{\omega_c}\right)^m}\frac{1}{G_f(s)}\,. \tag{37}$$

For a stable plant, this controller has a structure similar to the fractional PID controller defined by:

$$C_m(s) = K_c + \frac{K_i}{s^\lambda} + K_d s^\mu. \tag{38}$$

The open loop transfer function becomes:

$$G_0(s) = \left(K_c + \frac{K_i}{s^\lambda} + T_d s^\mu\right)\underbrace{\frac{K}{1+\tau s}}_{G_f(s)} = K_i\left(\frac{1+\dfrac{K_c}{K_i}s^\lambda + \dfrac{T_d}{K_i}s^{\lambda+\mu}}{s^\lambda}\right)\frac{K}{1+\tau s}\,. \tag{39}$$

$G_0(s)$ equal to the fractional order (33), so the controller (38) is designed in such a way that it compensates the process denominator by its numerator as following:

$K_c = 0$, $G_0(s)$ becomes:

$$G_0(s) = K_i\left(\frac{1+\dfrac{T_d}{K_i}s^{\lambda+\mu}}{s^\lambda}\right)\frac{K}{1+\tau s}\,. \tag{40}$$

From Eq. (40), we obtain the five parameters of the FOPID controller as follows:

$$\lambda = m; \quad K_i = \frac{\omega_c^m}{K}; \quad T_d = \tau K_i; \quad \mu = 1 - m. \tag{41}$$

4. Proposed robustness metric

After the presentation of the three analytical design techniques, it becomes evident that the iso-damping property can be achieved through various methods. However, these resulting closed-loop systems exhibit different levels of robustness, primarily depending on how closely their behavior aligns with the Bode's Ideal Transfer Function (BITF), which is inherently robust to static gain variations.

Therefore, to enable a meaningful comparison between these robust control strategies, it is essential to introduce a quantitative robustness index, analogous to the maximum sensitivity metric commonly used in classical robust control. In this work, a robustness degree is proposed to evaluate and quantify the resilience of the closed-loop system to static gain variations. The objective is to measure the proximity of the actual closed-loop frequency response to the ideal BITF model, thereby providing a consistent basis for robustness assessment in the frequency domain.

Inspired by the approach adopted in [9], where the authors utilized the integral square of phase difference between the actual and desired open-loop systems as a fitness function to optimize for robustness, we propose an enhanced approach. Specifically, we introduce a **frequency-domain robustness index** based on the integral of the absolute error (IAE) between the magnitude and phase responses of the actual open-loop transfer function and the ideal Bode's transfer function. Figure 5a illustrates the limited frequency range over which the error between the actual and desired open-loop responses is computed.

To emphasize accuracy near the gain crossover frequency ω_c, where robustness is most critical, a weighting function is applied to prioritize this region. In other words, it assigns greater importance to this frequency region ω_c. A Gaussian (normal) distribution is employed as the weighting function to achieve this objective (Fig. 5b).

Finally, the proposed robustness metric can be computed using the following equation:

$$I_x = IAE = \int_{\omega_{\min}}^{\omega_{\max}} H(\omega) * |\varepsilon(\omega)| \, \mathrm{d}\omega, \tag{42}$$

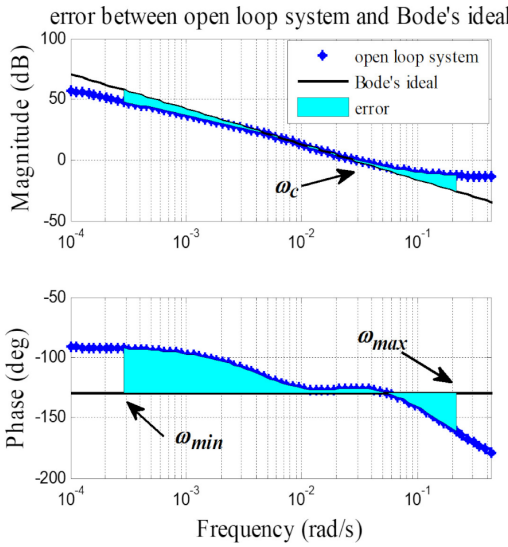

(a) Area between Bode's ideal function and open loop system

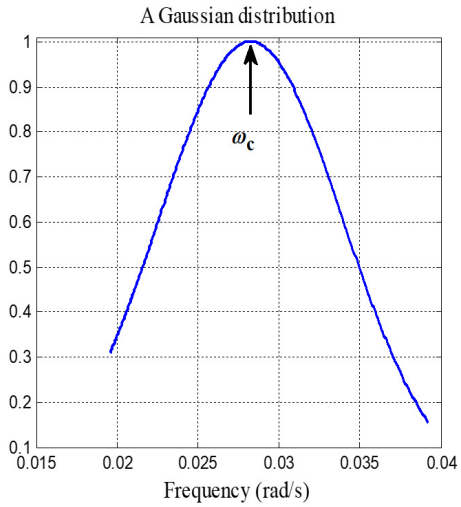

(b) Gaussian function used

Figure 5

with $H(\omega)$ is a Gaussian distribution centered at ω_c. $\varepsilon(\omega)$ denotes the difference between the magnitude and/or phase of the actual and desired open-loop response.

The colored region bounded by $\omega_{\min}$ and $\omega_{\max}$ frequencies represents a frequency band around the chosen ω_c. The proposed robustness index reaches its optimal value when this error is minimized, indicating that the system closely

resembles Bode's Ideal Transfer Function, particularly in terms of phase flatness near ω_c. It is also important to note that the magnitude slope plays a crucial role, as any variation in the system gain results in a shift of the gain crossover frequency ω_c along this slope.

5. Results

This study aims to validate the three controller design methods presented in Section 3 through both simulation and experimental implementation. The evaluation also includes the proposed robustness metric introduced in Section 4.

The main objective is to investigate the effect of time-delay on the preservation of the iso-damping property. On the one hand, it is well known that time-delay imposes fundamental performance limitations, notably described by the frequency crossover inequality proposed by Åström [17], which states that:

$$\left(\omega_c.\theta < \frac{\pi}{2}\right). \tag{43}$$

On the other hand, in [23], the authors used a novel time-delay approximation valid for:

$$(\omega_c.\theta < 0.5). \tag{44}$$

Once this inequality is considered during the controller design, the iso-damping propriety can be achieved using their tuning method.

The present study aims to examine, confirm, and experimentally validate whether this latter (Eq. (44)) condition represents a practical robustness limit imposed by time-delay in achieving iso-damping behavior. To carry out this study, the desired closed-loop specifications were fixed, and the time-delay value was incrementally increased using a software-based simulation. This approach allowed us to highlight the effect of the product $\theta.\omega_c$ on the preservation of the iso-damping property.

We consider the FOPTD system given by the Eq. (3).

The design specifications required for the controlled system are the following:

- Gain crossover frequency, $\omega_c = 0.028$ rad/s.
- Phase margin, $\emptyset_m = 50°$.
- Robustness to variations in the gain of the plant must be fulfilled.

Below are the different simulation and experimental results with the time-delay equal to 3 s. After that, we show different results for other time delays respectively: 8, 17 and 25 s.

5.1.

To satisfy the different specifications, the controllers parameters are shown in Table 2. These controllers are simulated using the Charef's approximation [31].

Table 2: Different parameters of controllers

	$\theta = 3$ s	$\theta = 8$ s
Method 1	$0.6571 + \frac{0.0144}{s^{1.01}} - 6.76s$	$0.7515 + \frac{0.0149}{s^{1.01}} - 2.62s$
Method 2	$22.724\left(\frac{1}{158.5s} + 1.4858s\right) * \left(\frac{1}{1+114.8157s^{0.44}}\right)$	$8.6559\left(\frac{1}{161s} + 3.9006s\right) * \left(\frac{1}{1+43.0559s^{0.44}}\right)$
Method 3	$\left(\frac{0.0012}{s^{1.444}} + 0.1933s^{-0.444}\right) * \frac{(1+3.0081s)}{1.0035(1+0.001s)}$	$\left(\frac{0.0012}{s^{1.444}} + 0.1933s^{-0.444}\right) * \frac{(1+8.1376s)}{1.0256(1+0.001s)}$
	$\theta = 17$ s	$\theta = 25$ s
Method 1	$0.8834 + \frac{0.0149}{s^{1.01}} + 4.74s$	$0.9543 + \frac{0.0146}{s^{1.01}} + 11.65s$
Method 2	$4.1872\left(\frac{1}{165.5s} + 8.0634s\right) * \left(\frac{1}{1+20.2616s^{0.44}}\right)$	$2.9161\left(\frac{1}{169.5s} + 11.5782s\right) * \left(\frac{1}{1+13.7779s^{0.44}}\right)$
Method 3	$\left(\frac{0.0012}{s^{1.444}} + 0.1933s^{-0.444}\right) * \frac{(1+18.4133s)}{1.1251(1+0.001s)}$	$\left(\frac{0.0012}{s^{1.444}} + 0.1933s^{-0.444}\right) * \frac{(1+30.0834s)}{1.3075(1+0.001s)}$

All three methods successfully meet the desired specifications, exhibiting a flat phase near the gain crossover frequency. However, as the time delay increases from 3 s, the phase flatness in the Bode diagram progressively degrades, as illustrated in Fig. 6.

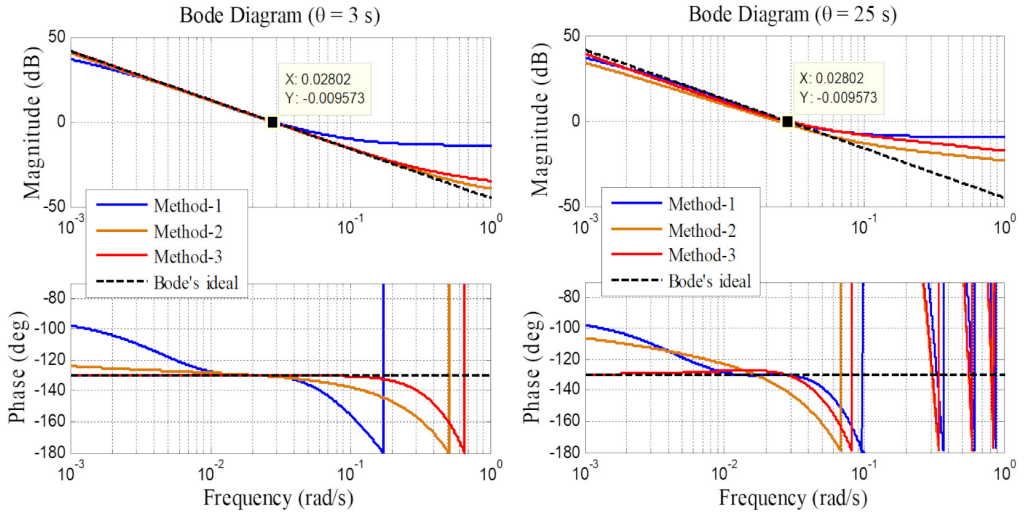

Figure 6: Bode plot of the open loop system

Figures 7 and 8 show respectively the obtained gain crossover frequency and phase margin using three tuning methods. It can be clearly observed that Methods 1 and 3 consistently achieve the two desired specifications, crossover

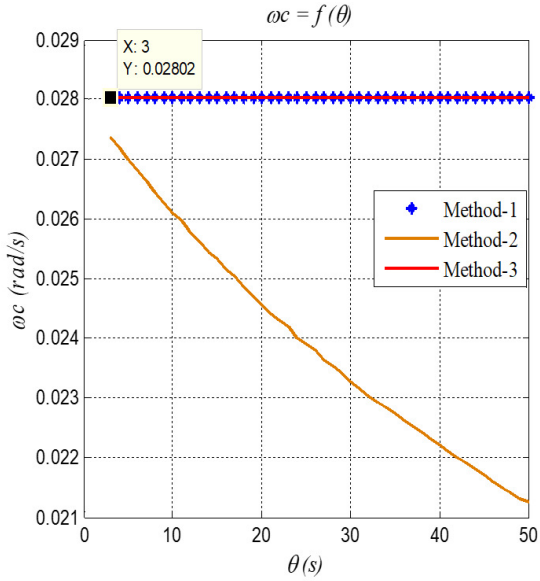

Figure 7: Crossover frequency ω_c with respect to θ

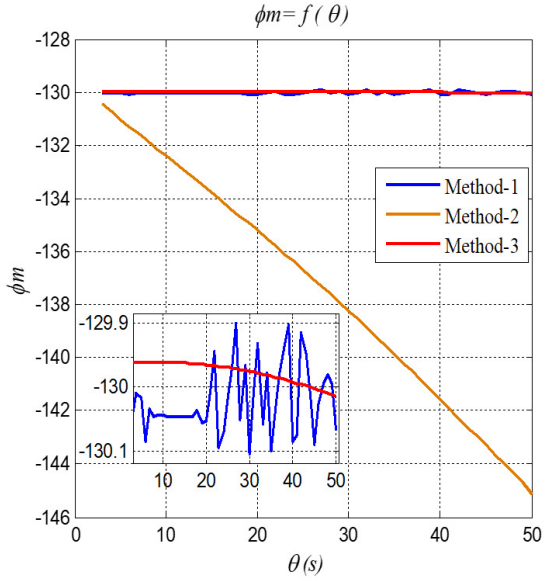

Figure 8: Phase margin with respect to θ

frequency ω_c and phase margin φ_m across all simulated values of time delay θ. In contrast, Method 2 shows a noticeable deviation from these target values as θ increases.

As shown in Fig. 9, all three controllers exhibit a near-zero phase derivative at the gain crossover frequency $\theta = 3s$, indicating iso-damping behavior. Method 1 maintains this flat-phase condition across a wide range, specifically for $\theta < 25s$. In contrast, Method 2 shows a linear degradation in phase flatness as θ increases. Although Method 3, like Method 1, is model-based, it initially achieves excellent flatness at $\theta = 3s$, but the phase slope progressively deteriorates with increasing time delay.

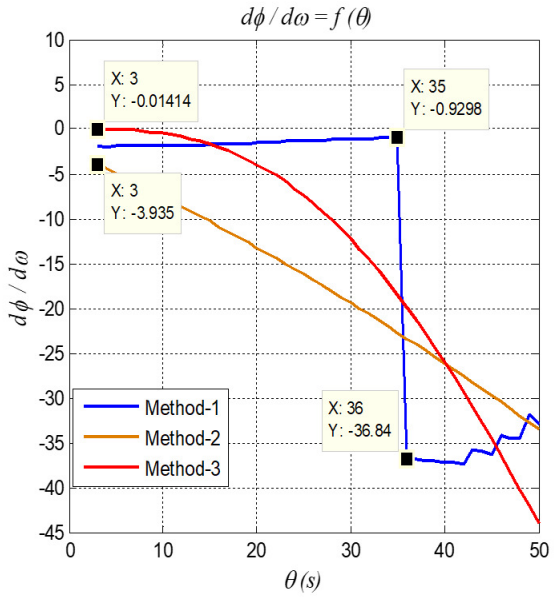

Figure 9: Phase derivative with respect to θ

Figure 10 presents the step responses of the closed loop system controlled by the three controllers under static gain variations namely, $[0.7, 1, 1.3, 2, 2.5, 3] * K_{\text{nominal}}$, considering two time-delay cases. The first one is $\theta = 3s$ where the iso-damping has been achieved for large gain variations especially with Method 2 and 3 (notably, the obtained step responses using Methods 2 and 3 closely match the desired reference response, although this desired response does not include time delay). The second one is that this property has been partially disappeared at $\theta = 25s$, indicating the sensitivity of robustness to increased time delay.

Despite all methods meeting the nominal performance specifications, the effect of time delay on the preservation of the iso-damping property differs significantly among them.

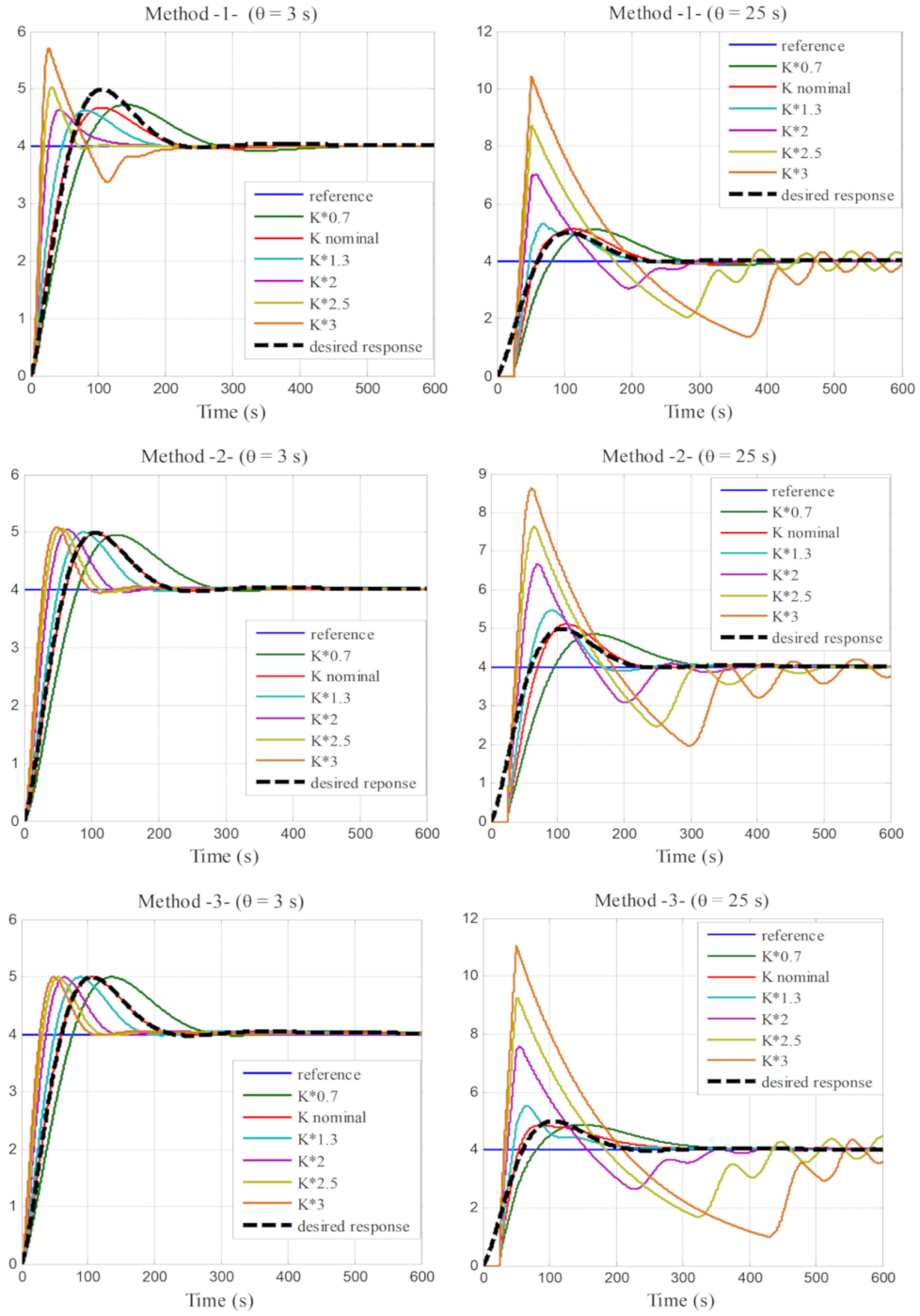

Figure 10: Simulation step response of the controlled system with different controllers and time delays

5.2. Experimental results

To validate the simulation results, experimental tests were conducted on the laboratory-scale, exactly on the liquid level control system described in Section 2. The same controller parameters and operating conditions used in the simulations were implemented to evaluate the performance of each method in real-time, particularly in terms of the iso-damping preservation or the robustness to static gain variations under different time delays.

The controllers listed in Table 2 were implemented using Charef's approximation method [31] with discrete state space representation at sampling time $T_s = 0.5$ s.

The experimental results obtained using the three controllers under different time-delay conditions are illustrated in Fig. 11.

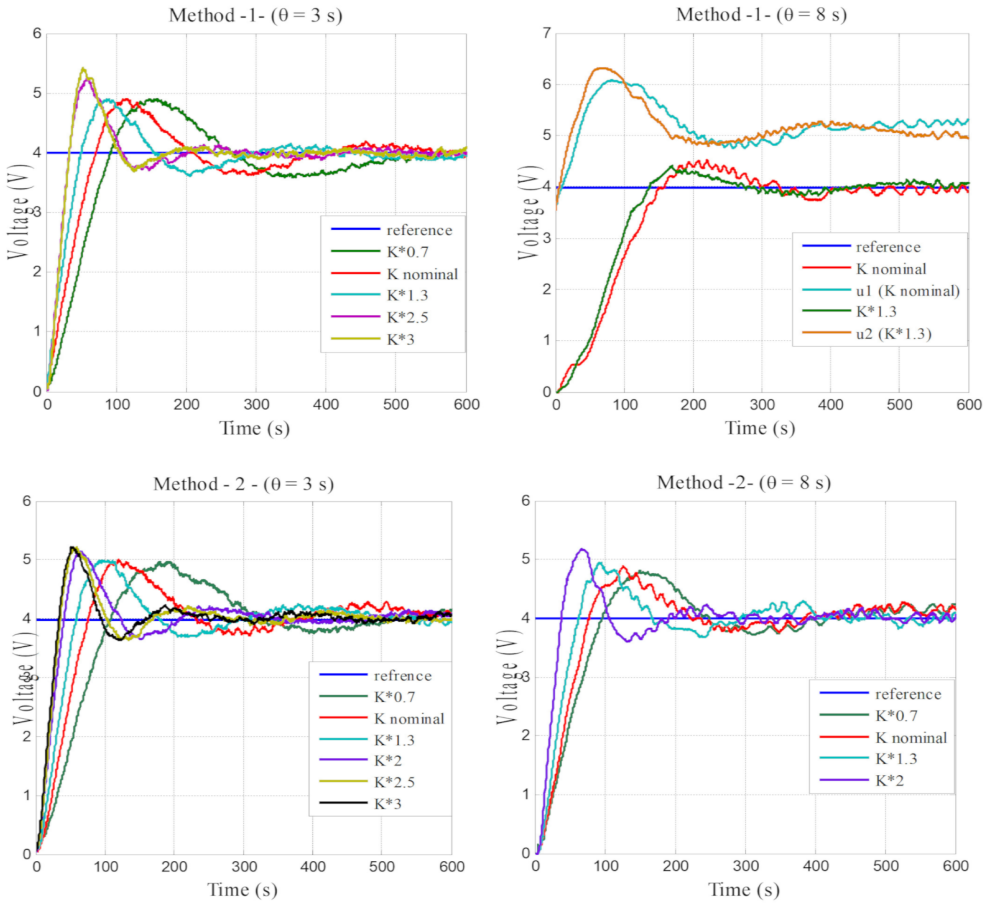

Fig. 11. Part 1

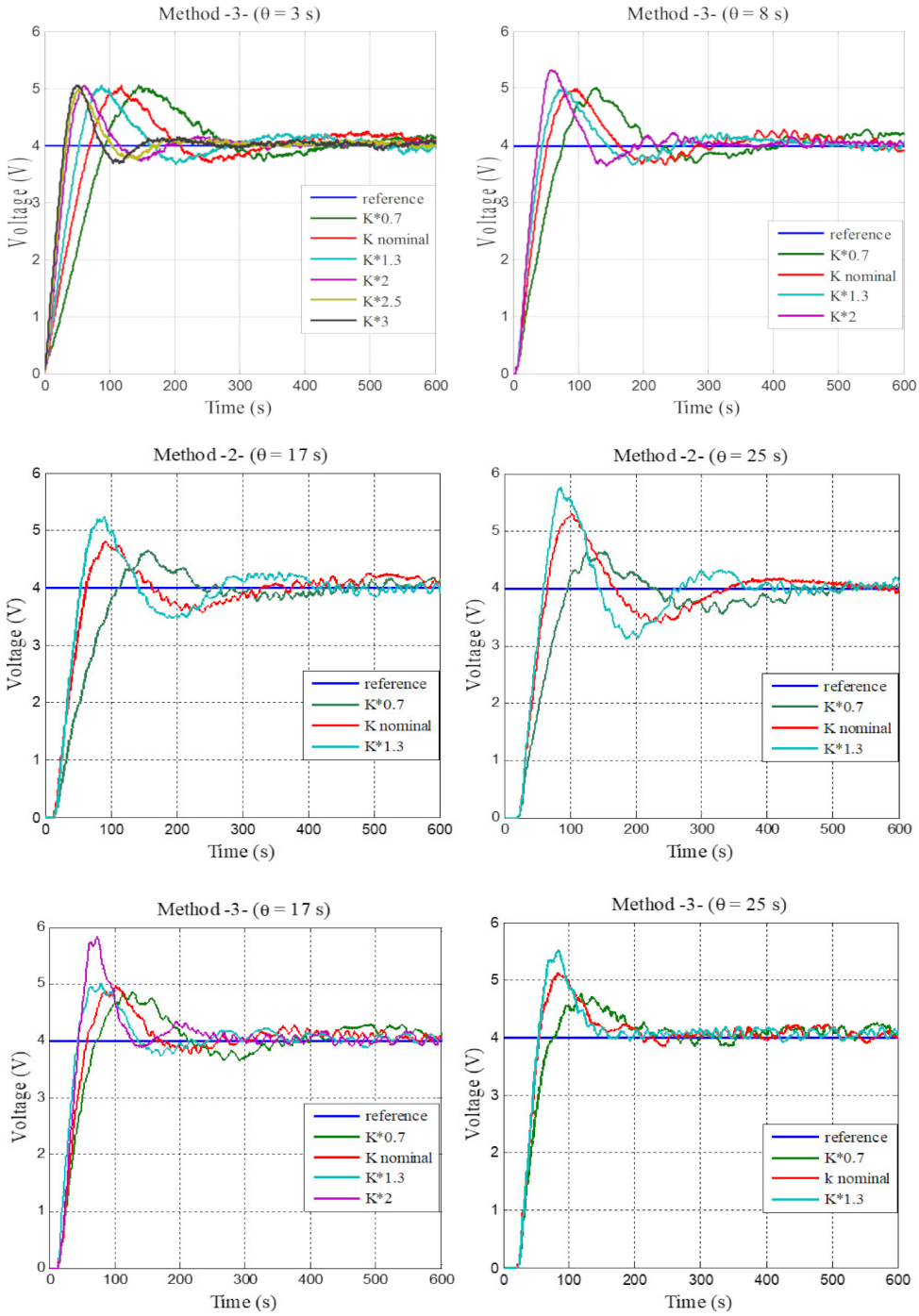

Figure 11: Experimental step response of the controlled system with different controllers under varying time delay conditions

For $\theta = 3s$, the controller designed using Method 3 achieved complete isodamping for all tested static gain variations, confirming the quality of the phase flatness observed in the Bode diagram (Fig. 6). In contrast, the controllers designed using Methods 1 and 2 began to lose robustness when the static gain exceeded twice the nominal value.

For $\theta = 8$ to 25 s

All methods produced controllers that partially lost their robustness properties as the time delay increased. However, the controller designed using Method 1 failed to satisfy the desired specifications starting from $\theta = 8s$. Controller 3 demonstrated both the best performance and robustness compared to Controller 2, which completely lost its robustness at $\theta = 17s$ (corresponding to $\omega_c \cdot \theta = 0.5$). In contrast, Controller 3 maintained robustness for static gain variations within the range of $[0.7, 1, 1.3, 2, 2.5, 3] * K_{\text{nominal}}$, but partially lost this robustness when the time delay increased to $\theta = 25$.

These results highlight the varying degrees of robustness among the controllers, emphasizing the need for a quantitative robustness metric. The figures

Table 3: Time and frequency characteristics $K_1 = 0.7 * K_{\text{nominal}}$

Desired values	Frequency characteristics			Time characteristics			
	$Ø_m$	ω_c	$dØ/d\omega$	t_s (10~90)		Overshoot (%)	
				simul.	exper.	simul.	exper.
$\theta = 3s$							
Method 1	50.34	0.0212	−0.3586	58.8	68.63	18.2	22.5
Method 2	50.23	0.0213	−4.4778	57.06	79.3	23.9	24.25
Method 3	**50.04**	**0.0219**	**−0.0059**	57.08	73.67	24.82	26
$\theta = 8s$							
Method 1	50.28	0.0214	−0.2153	53.45	–	20.97	–
Method 2	49.95	0.0205	−7.0967	57.74	69.16	23	20
Method 3	**50.1**	**0.0217**	**−0.1095**	54.58	53.85	24.77	25.25
$\theta = 17s$							
Method 1	**50.23**	**0.0213**	0.0806	48.867	–	23.82	–
Method 2	49.39	0.0191	−11.9603	57.387	3.39	21.87	17.25
Method 3	50.71	0.0212	**−1.0141**	48.89	43.76	24.05	21.75
$\theta = 25s$							
Method 1	**49.91**	**0.0210**	1.1643	43.42	–	27.7	–
Method 2	48.82	0.0180	−16.4999	55.73	57.63	21.37	16
Method 3	52.38	0.0203	**−3.0611**	41.84	34.68	21.87	18.5

also highlight the limitations of each controller in maintaining the iso-damping property as the time-delay increases.

A summary of simulation and experimental results, representing time-domain and frequency-domain characteristics, is presented in Tables 3, 4, and 5 for the three static gain values: $0.7 * K_{\text{nominal}}$, K_{nominal}, and $1.3 * K_{\text{nominal}}$, respectively.

Note: The normal distribution centered at the gain crossover frequency (ω_c = 0.028 rad/s). Furthermore, we have chosen the interval between $0.0196 \leqslant \omega \leqslant 0.0396$ rad/s.

It is clearly observed that Controller 3 exhibits the lowest robustness index I_x and also achieves the best performance values compared to the other controllers in the most of the tests. This controller satisfies high accuracy in meeting the desired specifications and maintains phase flatness, as indicated by the low value of $d(\arg)/d\omega$ in Table 4. This property is preserved for $\theta \leqslant 17$, but is lost for higher time-delay values across all three controllers.

Table 4: Time and frequency characteristics $K_2 = K_{\text{nominal}} = K$

Desired values	Frequency characteristics				Time characteristics			
	$Ø_m$	ω_c	$dØ/d\omega$	I_x	t_s (10~90)		Overshoot (%)	
					simul.	exper.	simul.	exper.
	50°	0.028 rad	0	0	t_s = 44 s		24.8%	
$\theta = 3s$								
Method 1	49.93	**0.028**	−1.9196	0.0098	41.9	53.83	16.1	22.5
Method 2	49.54	0.0274	−3.9347	0.0121	44	54.5	24.5	25.25
Method 3	**50.04**	**0.028**	**−0.0141**	**1.555e − 04**	**44**	**54.48**	**24.82**	**25.25**
$\theta = 8s$								
Method 1	49.91	**0.028**	−1.9068	0.0091	37.55	114.9	20.95	13
Method 2	48.16	0.0265	−6.5458	0.0409	**43.34**	**55.97**	24.62	22
Method 3	**50.04**	**0.028**	**−0.2656**	0.0016	41.18	36.36	**24.77**	**22**
$\theta = 17s$								
Method 1	49.96	**0.028**	**−1.6831**	0.0086	33.17	–	24.67	–
Method 2	45.64	0.025	−11.4841	0.1017	**40.35**	**37.58**	25.6	20
Method 3	**50.037**	**0.028**	−2.4591	0.0107	32.2	32.78	**23.95**	**24.25**
$\theta = 25s$								
Method 1	49.94	**0.028**	**−1.3451**	0.0102	26.7	–	28.17	–
Method 2	43.30	0.0239	−16.2394	0.1651	**36.65**	**32.56**	27.9	32.25
Method 3	**50.03**	**0.028**	−7.4147	0.0283	23.26	23.73	**20.77**	**27.5**

Table 5: Time and frequency characteristics $K_3 = 1.3 * K_{\text{nominal}}$

Desired values	Frequency characteristics			Time characteristics			
	Ø_m	ω_c	$d\text{Ø}/d\omega$	t_s (10~90)		Overshoot (%)	
				simul.	exper.	simul.	exper.
$\theta = 3s$							
Method 1	48.76	0.0351	−3.7456	31.26	39.28	15.57	22.37
Method 2	48.95	**0.0329**	−3.5934	36.28	41.38	25	25
Method 3	**50.034**	0.0336	**−0.0234**	36.28	40.89	24.82	26.25
$\theta = 8s$							
Method 1	48.79	0.0347	−3.8644	27.94	90.6	21.25	10
Method 2	46.60	**0.0320**	−6.2067	34.87	43.13	26.07	23.75
Method 3	**49.92**	0.0338	**−0.4372**	33.03	29.57	24.77	24.5
$\theta = 17s$							
Method 1	**48.89**	0.0348	**−3.7840**	23.35	–	25.5	–
Method 2	42.29	**0.0305**	−11.2613	30.45	29.65	29.6	30.75
Method 3	48.77	0.0349	−3.9638	21.8	23.14	23.85	25
$\theta = 25s$							
Method 1	**48.49**	0.0359	**−5.0335**	19.35	–	32.55	–
Method 2	38.13	**0.0295**	−16.2858	26.55	28.9	36.75	44
Method 3	45.25	0.0368	−11.4726	17.07	22.67	38.25	38

6. Concusions

This work has investigated the preservation of the iso-damping property in fractional-order control systems subjected to time delays through a comparative analysis of three analytical design methods. New frequency-domain robustness metric was introduced to quantify the degree of iso-damping by measuring the proximity of the open-loop response to the Bode's Ideal Transfer Function (BITF). Simulation and experimental validation were carried out using a liquid level process, and the results revealed the effect of time-delay on phase flatness and robustness under static gain variations.

Among the evaluated methods, the third approach demonstrated superior robustness and maintained the iso-damping behavior over a wider range of time delays and gain variations. Controller 2 exhibited a loss of robustness beyond a specific delay threshold, confirming the performance degradation by the product of $\theta.\omega_c$ constraint.

Controller 1 showed intermediate performance with early deviations from desired specifications.

All the presented results confirm the inherent trade-off between system bandwidth and the achievement of the iso-damping property, particularly under the condition $\theta.\omega_c < 0.5$, which appears as a critical threshold for maintaining phase flatness and robustness. In this context, the need to ensure the iso-damping behavior inherently leads to a reduction in system bandwidth through limiting the crossover frequency. This underscores the necessity of carefully balancing performance and robustness in the design of controllers for time-delay systems.

References

[1] A. Oustaloup: *La commande CRONE: commande robuste d'ordre non entier*. Hermes, 1991.

[2] I. Polubny: Fractional-order systems and PIλDμ controller. *IEEE Transactions on Automatic Control*, **44** (1999), 208–214. DOI: 10.1109/9.739144

[3] P. Shah and S. Agashe: Review of fractional PID controller. *Mechatronics*, **38** (2016), 29–41. DOI: 10.1016/j.mechatronics.2016.06.005

[4] I. Birs, C. Muresan, I. Nascu, and C. Ionescu: A survey of recent advances in fractional order control for time delay systems. *IEEE Access*, **7** (2019), 30951–30965. DOI: 10.1109/ACCESS.2019.2902567

[5] R. Caponetto, G. Maione, and J. Sabatier: Fractional-order control: A new approach for industrial applications, *Control Engineering Practice*, **56** (2016), 157–158. DOI: 10.1016/j.conengprac.2016.09.008

[6] R.S. Barbosa, J.T. Machado, and I.M. Ferreira: Tuning of PID controllers based on Bode's ideal transfer function. *Nonlinear dynamics*, **38** (2004), 305–321. DOI: 10.1007/s11071-004-3763-7

[7] R.S. Barbosa, M.F. Silva, and J.T. Machado: Tuning and application of integer and fractional order PID controllers. In *Intelligent Engineering Systems and Computational Cybernetics*, Ed: Springer, 2009, 245–255. DOI: 10.1007/978-1-4020-8678-6_21

[8] C.A. Monje, B.M. Vinagre, V. Feliu, and Y. Chen: Tuning and auto-tuning of fractional order controllers for industry applications. *Control Engineering Practice*, **16** (2008), 798–812. DOI: 10.1016/j.conengprac.2007.08.006

[9] B. Saidi, M. Amairi, S. Najar, and M. Aoun: Bode shaping-based design methods of a fractional order PID controller for uncertain systems. *Nonlinear Dynamics*, 80 (2015), 1817–1838. DOI: 10.1007/s11071-014-1698-1

[10] B. Maamar and M. Rachid: IMC-PID-fractional-order-filter controllers design for integer order systems. *ISA Transactions*, **53** (2014), 1620–1628. DOI: 10.1016/j.isatra. 2014.05.007

[11] P. Chen, Y. Luo, Y. Peng, and Y. Chen: Optimal robust fractional order PIλD controller, synthesis for first order plus time delay systems. *ISA Transactions*, **114** (2021), 136–149. DOI: 10.1016/j.isatra.2020.12.043

[12] N. Fergani and A. Charef: Process step response based fractional PIλDμ controller parameters tuning for desired closed loop response. *International Journal of Systems Science*, **47** (2016), 521–532. DOI: 10.1080/00207721.2014.891667

[13] P. Chen and Y. Luo: An analytical synthesis of fractional order PIλDμ controller design. *ISA Transactions*, **131** (2022), 124–136. DOI: 10.1016/j.isatra.2022.04.047

[14] SKC, *Network Analysis and Feedback Amplifier Design*, Ed: JSTOR, 1948.

[15] Y. Luo and Y. Chen: Fractional order [proportional derivative] controller for a class of fractional order systems. *Automatica*, **45** (2009), 2446–2450. DOI: 10.1016/j.automatica.2009.06.022

[16] H. Li, Y. Luo, and Y. Chen: A fractional order proportional and derivative (FOPD) motion controller: tuning rule and experiments. *IEEE Transactions on Control Systems Technology*, **18** (2009), 516–520. DOI: 10.1109/TCST.2009.2019120

[17] K.J. Åström: Limitations on control system performance. *European Journal of Control*, **6** (2020), 2–20. DOI: 10.1016/S0947-3580(00)70906-X

[18] Y. Chen, C. Hu, and K.L. Moore: Relay feedback tuning of robust PID controllers with iso-damping property. In *42nd IEEE international conference on decision and control (IEEE Cat. No. 03CH37475)*, 2003, 2180–2185. DOI: 10.1109/CDC.2003.1272941

[19] Y. Luo and Y. Chen: Stabilizing and robust fractional order PI controller synthesis for first order plus time delay systems. *Automatica*, **48** (2012), 2159–2167. DOI: 10.1016/j.automatica.2012.05.072

[20] S. Saha, S. Das, R. Ghosh, B. Goswami, R. Balasubramanian, A. Chandra, S. Das, and A. Gupta: Fractional order phase shaper design with Bode's integral for iso-damped control system. *ISA Transactions*, **49** (2010), 196–206. DOI: 10.1016/j.isatra.2009.12.001

[21] L. Liu, S. Zhang, D. Xue, and Y.Q. Chen: General robustness analysis and robust fractional-order PD controller design for fractional-order plants. *IET Control Theory & Applications*, **12**, (2018), 1730–1736. DOI: 10.1049/iet-cta.2017.1145

[22] S. Chen and H. Huang: Design of fractional order proportional integral controller using stability and robustness criteria in time delay system. *Measurement and Control*, **52** (2019), 1552–1566. DOI: 10.1177/0020294019877513

[23] N. Fergani, N. Boutasseta, and I. Attoui: An explicit tuning of the fractional order controller using a novel time delay approximation. *International Journal of Dynamics and Control*, **11** (2023), 2410–2422. DOI: 10.1007/s40435-023-01132-6

[24] S. Wang, P. Huang, Y. Luo, X. Wang, and X. Luo: A fractional-order ADRC with improved robustness to plant gain variations. *IEEE Transactions on Industrial Electronics*, 2025. DOI: 10.1109/TIE.2025.3552274

[25] E. Yumuk, M. Güzelkaya, and İ. Eksin: Analytical fractional PID controller design based on Bode's ideal transfer function plus time delay. *ISA transactions*, **91** (2019), 196–206. DOI: 10.1016/j.isatra.2019.01.034

[26] P. Roy and B.K. Roy: Fractional order PI control applied to level control in coupled two tank MIMO system with experimental validation. *Control Engineering Practice*, **48** (2016), 119–135. DOI: 10.1016/j.conengprac.2016.01.002

[27] S. K. Vavilala and V. Thirumavalavan: Level control of a conical tank using the fractional order controller. *Computers & Electrical Engineering*, **87** (2020). DOI: 10.1016/j.compeleceng.2020.106690

[28] R. Arivalahan, P. Tamilarasan, and M. Kamalakannan: Liquid level control in two tanks spherical interacting system with fractional order proportional integral derivative controller using hybrid technique: A hybrid technique/ *Advances in Engineering Software*, **175** (2023). DOI: 10.1016/j.advengsoft.2022.103316

[29] M. Allad and D. Acheli: Liquid level cascade control using various combinations of controllers. *Revue Roumaine des Sciences Techiniques – série Electrotechnique et Enérgetique*, **63** (2018), 94–99.

[30] M. Charif, M. Allad, and M.O. Bensidhoum: Implementation of simple fuzzy PI controller for liquid level cascade control. *Journal Européen des Systèmes Automatisés*, **57** (2024). DOI: 10.18280/jesa.570303

[31] A. Charef: Analogue realisation of fractional-order integrator, differentiator and fractional PIλDμ controller. *IEE Proceedings-Control Theory and Applications*, **153** (2006), 714–720. DOI: 10.1049/ip-cta:20050019